Lifetime and polarization of the radiative decay of excitons, biexcitons, and trions in CdSe nanocrystal quantum dots

Marco Califano,[1,2] Alberto Franceschetti,[2] and Alex Zunger[2]
[1]*Institute of Microwaves and Photonics, School of Electronic and Electrical Engineering, University of Leeds, Leeds LS2 9JT, United Kingdom*
[2]*National Renewable Energy Laboratory, Golden, Colorado 80401, USA*
(Received 5 May 2006; revised manuscript received 30 October 2006; published 1 March 2007)

Using the pseudopotential configuration-interaction method, we calculate the intrinsic lifetime and polarization of the radiative decay of single excitons (X), positive and negative trions (X^+ and X^-), and biexcitons (XX) in CdSe nanocrystal quantum dots. We investigate the effects of the inclusion of increasingly more complex many-body treatments, starting from the single-particle approach and culminating with the configuration-interaction scheme. Our configuration-interaction results for the size dependence of the single-exciton radiative lifetime at room temperature are in excellent agreement with recent experimental data. We also find the following. (i) Whereas the polarization of the *bright* exciton emission is always perpendicular to the hexagonal c axis, the polarization of the *dark* exciton switches from perpendicular to parallel to the hexagonal c axis in large dots, in agreement with experiment. (ii) The ratio of the radiative lifetimes of mono- and biexcitons $\tau(X):\tau(XX)$ is $\sim 1:1$ in large dots ($R=19.2$ Å). This ratio increases with decreasing nanocrystal size, approaching 2 in small dots ($R=10.3$ Å). (iii) The calculated ratio $\tau(X^+):\tau(X^-)$ between positive and negative trion lifetimes is close to 2 for all dot sizes considered.

DOI: 10.1103/PhysRevB.75.115401 PACS number(s): 71.15.−m, 71.55.−i

I. INTRODUCTION

Optically generated excitons in nanocrystal quantum dots (NQDs) can exist as neutral monoexcitons X (one electron, one hole, or e-h), charged excitons X^+ (e-$2h$) or X^- ($2e$-h), biexcitons XX ($2e$-$2h$), etc. (see Fig. 1). Previous experimental studies have shown[1] that the decay of XX in CdSe NQDs occurs on a fast, sub-100-ps time scale due to efficient *nonradiative* Auger recombination, compared to the ~20 ns time scale for the *radiative* decay of X. Fast Auger lifetimes were indeed predicted[2] for X^+, X^-, and XX in CdSe NQDs. The efficiency of the nonradiative Auger process is evidenced by the fact that injection of additional electrons into the quantum confined states of CdSe nanocrystals leads[3] to a quenching of the photoluminescence (PL). As a result, radiative e-h recombination is undetectable in *time-integrated* PL experiments. A signature of the radiative decay of XX has only recently been observed[4] as a low-energy shoulder of the monoexciton PL peak using *time-resolved*, femtosecond PL measurements. The situation is different for CdSe/ZnSe self-assembled quantum dots, where, due to a less efficient nonradiative (Auger) recombination mechanism, the lifetimes for the radiative decay of X, X^-, and XX have been measured.[5] The ratio between exciton and biexciton radiative lifetimes was found to be[5] $\tau(X):\tau(XX)\sim 2:1$.

In this paper, using the pseudopotential configuration-interaction (CI) method, we will address the radiative lifetime and the polarization of the band-edge emission of excitons, charged excitons, and biexcitons in CdSe colloidal quantum dots.

Radiative lifetimes. Calculating the radiative lifetimes of excitonic and multiexcitonic states is interesting from a theoretical standpoint because it allows one to determine the effects of the presence of additional carriers (with or without a total net charge) on the radiative recombination of an electron-hole pair. We find that in large CdSe dots ($R=19.2$ Å) the ratio between the lifetimes of the exciton and the biexciton bright states[6] is $\tau(X):\tau(XX)\sim 1:1$, which increases with decreasing size, approaching 2:1 in small dots ($R=10.3$ Å). Our calculated ratio $\tau(X^+):\tau(X^-)$ is also close to 2 for all dot sizes considered here. Another interesting question is the size dependence of the monoexciton radiative lifetime. We will compare our results with recent experimental results, which show an increase of the radiative lifetime with the dot size. We will also discuss the role of correlation effects in determining the size dependence of the radiative lifetime.

Polarization of band-edge emission. Electron-hole exchange interactions split the lowest excitonic manifold of CdSe quantum dots into a lower-energy, dark exciton (with a long radiative lifetime) and a higher-energy, bright exciton. We find that emission from the bright exciton is always polarized perpendicular to the wurtzite c axis for all dot sizes considered here. In the case of the emission from the dark exciton, we will show that correlation effects, introduced via configuration interaction, lead in large dots to a *rotation* of the polarization from perpendicular to parallel to the wurtzite c axis.

The paper is structured as follows: After a brief overview of our theoretical approach, we introduce the electronic structure of single excitons, positive and negative trions, and biexcitons, both in the single-particle picture and in the many-particle picture. We then discuss the evolution of energy levels, intrinsic radiative lifetimes, and polarization of the band-edge transitions of the single exciton through increasingly more complex many-body treatments, starting from the single-particle approach and culminating with the full-CI method. We then compare the calculated size dependence of the X radiative lifetime with recent experimental data. Finally, we discuss the radiative lifetime and polariza-

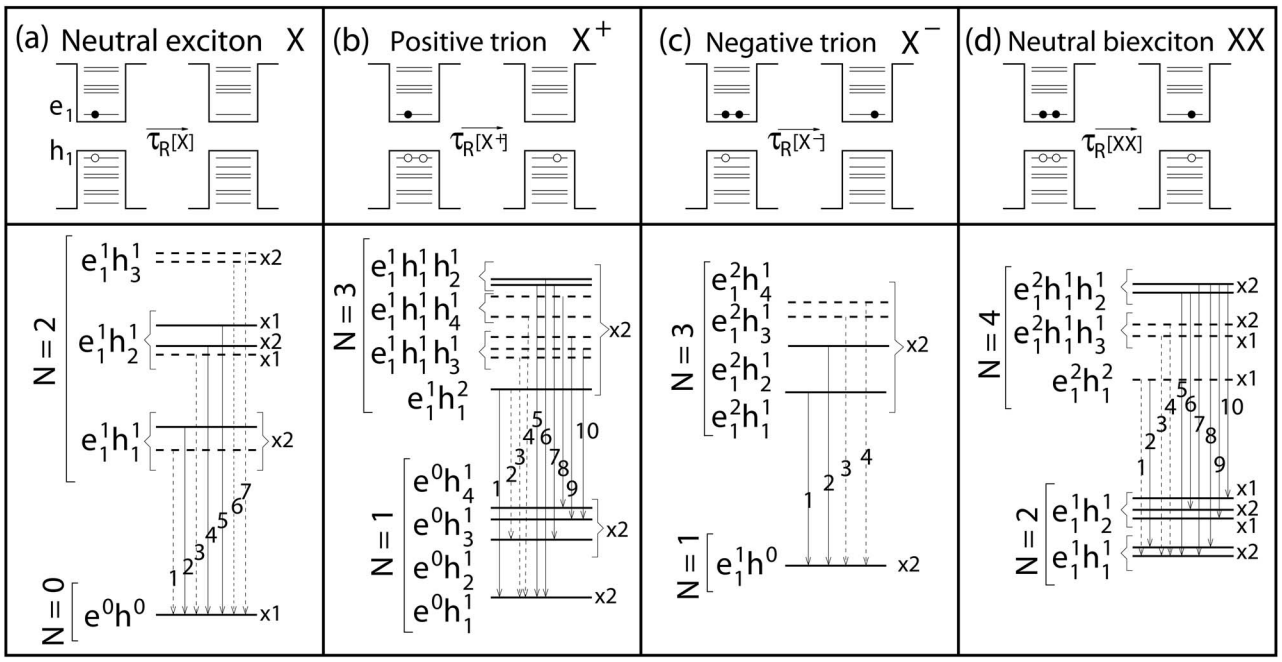

FIG. 1. Schematics of our calculated single-particle (upper panels) and excitonic (lower panels) levels for (a) neutral exciton X, (b) positive trion X^+, (c) negative trion X^-, and (d) neutral biexciton XX. Whereas the order of the excitonic levels in the lower panel is accurate, the energy scale is schematic. In the lower panel, the notation $(e_i^m h_j^n)$ indicates that a specific exciton level derives mainly from the single-particle levels e_i and h_j, occupied by m and n particles, respectively. The total number of particles is denoted by $N=n+m$. Also, "$\times p$" indicates an excitonic level degeneracy. The solid (dashed) horizontal lines indicate bright (dark) excitons, whereas the vertical arrows indicate transitions between levels. The numbers on these arrows label the transitions shown in Fig. 4.

tion of biexcitons (XX) and charged excitons (X^+ and X^-).

II. METHOD

We consider here three CdSe wurtzite spherical dots of radii $R=10.3$, 14.6, and 19.2 Å, whose surfaces are passivated by ligand potentials.[7] The single-particle energies ε_i and wave functions ψ_i are computed using the semiempirical, nonlocal pseudopotential method described in Refs. 8 and 9. The pseudopotential is derived from bulk local-density approximation (LDA) calculations and is adjusted to remove LDA errors in band gaps and effective masses. The single-particle Schroedinger equation is solved using a plane-wave basis set and including spin-orbit coupling. The excitonic wave functions $\Psi^{(i)}$ are then expanded in terms of single-substitution Slater determinants $\Phi_{v,c}$ constructed from the single-particle conduction (c) and valence (v) wave functions:

$$\Psi^{(i)} = \sum_{v=1}^{N_v} \sum_{c=1}^{N_c} C_{v,c}^{(i)} \Phi_{v,c}. \quad (1)$$

The many-body Hamiltonian is solved within the framework of the CI scheme, where we use a position-dependent screening for the Coulomb and exchange integrals. More details on the CI method can be found in Ref. 9. In the present work, the Slater determinants are built using $N_v=30$ valence states and $N_c=7$ conduction states, corresponding to CI basis sets of 840 configurations for the monoexciton, 5460 configurations for the negative trion, 24 780 for the positive trion, and 161 070 configurations for the biexciton. In our approach, the effects of charged carriers (electrons and holes) on the electronic structure are accounted for by the many-particle CI expansion. Figure 2 shows, for both X and XX, the CI convergence of the radiative lifetimes and energies of the transitions labeled 2 in Figs. 1(a) and 1(d). We see that the lifetime converges with a basis set of 15 valence states and 4 conduction states, while the convergence of the energy is slower.

The radiative lifetime for the transition $\Psi^{(i)} \rightarrow \Psi^{(j)}$ is obtained in the framework of standard time-dependent perturbation theory:[10]

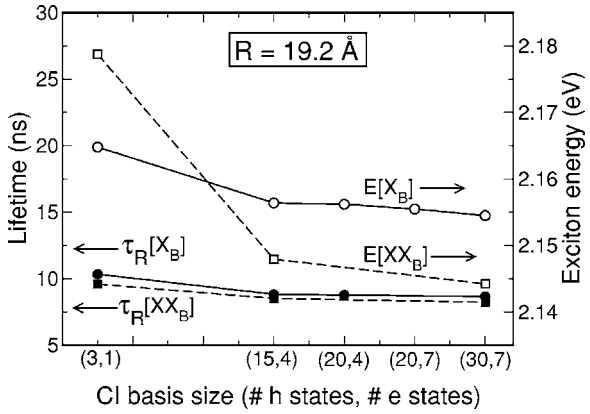

FIG. 2. Convergence with the CI basis set of the radiative lifetime and transition energy for transition 2 in Fig. 1(a) (X_B) and transition 2 in Fig. 1(d) (XX_B).

$$\left(\frac{1}{\tau}\right)_{i,j} = \frac{4nF\alpha\omega_{ij}^3}{3c^2}|\boldsymbol{M}_{i,j}|^2, \tag{2}$$

where n is the refractive index of the medium surrounding the nanocrystal, $F=3\varepsilon/(\varepsilon_{\mathrm{NQD}}+2\varepsilon)$ is the screening factor (here, $\varepsilon=n^2$ and $\varepsilon_{\mathrm{NQD}}$ is the dielectric constant of the NQD), α is the fine structure constant, $\hbar\omega_{ij}$ is the transition energy, c is the speed of light in the vacuum, and $\boldsymbol{M}_{i,j}$ is the CI dipole matrix element. In the case of a single exciton, for example, we have

$$\boldsymbol{M}_{i,j} = \sum_{v,c} C_{v,c}^{*(i)} C_{v,c}^{(j)} \langle \psi_v | \boldsymbol{r} | \psi_c \rangle, \tag{3}$$

where the coefficients $C_{v,c}^{(i)}$ are given by Eq. (1). The dielectric constant of the dot is calculated using a modified Penn model; we find $\varepsilon_{\mathrm{NQD}}=4.8$ for $R=10.3$ Å, 5.3 for $R=14.6$ Å, and 5.6 for $R=19.2$ Å. Here, we use the refractive index of toluene ($n=1.496$). This choice allows us to discuss the behavior of τ in realistic systems (typically, n ranges[11] from 1.375 for hexane to 1.496 for toluene), without, however, losing generality. Indeed, it has recently been found experimentally[12] that the influence of the solvent refractive index on the PL lifetime of CdSe NQDs is small, consistent with the observed[13] insensitivity of the absorption cross section of CdSe NQDs on the solvent refractive index.

The polarization of the emitted light is determined according to

$$P_\beta = \frac{I_\beta}{I_\perp + I_\parallel}, \tag{4}$$

where $\beta=\parallel,\perp$ and $I_\parallel, I_\perp$ are the intensities of the emitted light along the nanocrystal z axis (oriented along the c axis of the wurtzite lattice structure) and perpendicular to it, respectively.

III. RESULTS

A. From the single-particle level ladder to the many-particle excitonic ladder

Figure 1 (upper panels) shows schematically the single-particle levels of CdSe NQDs occupied by $N=2$, 3, and 4 particles. They are labeled as e_i and h_i, where $i=1,\ldots n$ increases from the valence-band maximum (h_1) to lower-energy levels and from the conduction-band minimum (e_1) to higher-energy levels. The envelope functions of the first four hole states h_1–h_4 have, respectively, s, s, p, and p angular momentum component, whereas the first two electron states e_1 and e_2 have mostly s and p characters, respectively. The lowest-energy excitonic states studied here derive from combinations of the uppermost four hole states h_1–h_4 and the lowest electron state e_1. As the energy separation between e_1 and e_2 is of the order of 300 meV for a $R=19.2$ Å CdSe NQD, and increases to about 600 meV for a $R=10.3$ Å dot, excitons derived from electron states higher than e_1 are highly excited, and therefore will not be considered in this work (they are, however, included in the expansion of the many-particle wave functions). The lower panel of Fig. 1 shows a schematic diagram of the calculated excitonic ladder.

B. Many-body effects on the transition energies and radiative lifetimes of neutral single excitons

We will analyze the excitonic energies and radiative decay times by decomposing the final CI results into four simple, physically recognizable terms, each corresponding to a different level of many-body treatment (denoted as LMT 1–LMT 4, in order of increasing level of sophistication).

(1) The single-particle level (LMT 1), where only the eigenvalues ε_i and the corresponding eigenfunctions ψ_i are used. Interelectronic Coulomb, exchange, and correlation effects are neglected. The excitons have no binding and are highly degenerate.

(2) Addition of the screened electron-hole direct Coulomb integrals (LMT 2). This perturbative correction leads to binding of the excitons and to spectral redshifts.

(3) The single-configuration level (LMT 3), in which Coulomb and exchange interactions within a single excitonic multiplet (e_ih_j) (single configuration) are included, but the interaction between different configurations is omitted. This leads to excitonic level splittings and to a lowering of the degeneracies.

(4) The full-CI level (LMT 4), which includes correlations as well as intraconfiguration Coulomb and exchange interactions. Here, all the configurations in the CI expansion are allowed to interact. All interelectronic direct and exchange Coulomb integrals are screened (Bethe-Salpeter approach).

Our results are as follows.

(1) At the single-particle level (LMT 1), all single-exciton states X are fourfold degenerate due to Kramer's degeneracy of the single-particle states. The two lowest exciton levels are derived, respectively, from (e_1h_1) and from (e_1h_2), and are both optically active (large oscillator strength). The next two exciton levels are derived from (e_1h_3) and (e_1h_4). Due to the different symmetries of the electron and hole envelope functions, they are optically inactive (small oscillator strength). From Fig. 3(a), we see that at the single-particle level the exciton radiative lifetime $\tau(X)$ decreases as the band gap increases, i.e., as the size is reduced. This is due to the factor $\tau^{-1}\propto\omega_{ij}^3$ in Eq. (2), which overcomes the decrease of the dipole matrix elements $|\boldsymbol{M}_{i,j}|^2$ with increasing gap [Fig. 3(b)], leading to an overall decrease of $\tau(X)$ with $E_g=\hbar\omega$.

(2) Adding the electron-hole Coulomb interaction to the single-particle approximation leads to a (level-dependent) shift of all excitonic levels (and consequently of the energy gap) to lower energies. This shift, which decreases with increasing NQD size from ~400 meV for a $R=10.3$ Å dot to ~200 meV for a $R=19.2$ Å dot, leaves the degeneracy of the levels, the allowed/forbidden character of the optical transitions, and the dipole matrix elements $\boldsymbol{M}_{i,j}$ unchanged. However, the dependence of the lifetime on the transition energy ω in Eq. (2) leads to a size-dependent increase in $\tau(X)$, when compared to the single-particle level (LMT 1). According to Eq. (2), we have

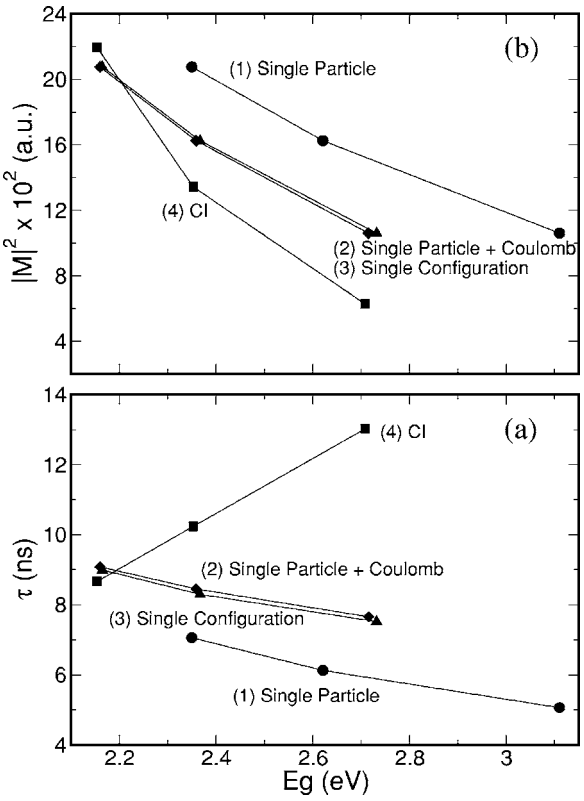

FIG. 3. Dependence of (a) the radiative lifetime and (b) the dipole matrix elements on the energy gap, for different levels of complexity in the many-body treatment for the lowest-energy optically allowed transition of the monoexciton X at zero temperature: (1) single particle (LMT 1), (2) single particle plus electron-hole direct Coulomb attraction (LMT 2), (3) single configuration (LMT 3), and (4) full configuration interaction (LMT 4). We plot consistently $\tau^{(L)}(X_B)$ and $|M^{(L)}(X_B)|^2$ vs $E_g^{(L)}$, where $L=1-4$ represents the many-body level.

$$\tau^{(\mathrm{SP+C})} = \left(\frac{E_g^{(\mathrm{SP})}}{E_g^{(\mathrm{SP+C})}}\right)^3 \tau^{(\mathrm{SP})}, \tag{5}$$

where "SP" and "SP+C" stand for single particle (LMT 1) and single particle+Coulomb (LMT 2), respectively. Thus, the inclusion of electron-hole interactions results in an increase of the lifetime by a factor $(E_g^{(\mathrm{SP})}/E_g^{(\mathrm{SP+C})})^3$, ranging from 1.5 for the smallest dot (where τ increases from 5.1 to 7.6 ns) to ~1.3 for the largest dot (where τ increases from 7 to 9 ns). As shown in Fig. 3(a), where τ and the relative E_g are calculated consistently within the same many-body approach (i.e., $\tau^{(\mathrm{SP})}$ is plotted vs $E_g^{(\mathrm{SP})}$), the radiative lifetime in this approximation still shows an increase with nanocrystal size.

(3) In the single-configuration approximation (LMT 3) Coulomb and exchange matrix elements between states within a single excitonic configuration are taken into account. The lowest exciton manifold—derived from the configuration (e_1h_1)—splits[9] into two twofold degenerate states (Fig. 1, lower panel): a lower-energy, nearly spin-forbidden dark state X_D (denoted by a dashed line in Fig. 1), and a higher-energy, optically allowed bright state X_B (solid line). Their radiative recombination transitions are labeled 1 and 2 in the lower panel of Fig. 1(a). X_D and X_B are separated by the exchange splitting energy Δ_{ex}, ranging in energy from ~5 to ~16 meV for dots with sizes $R=19.2-10.3$ Å. Above the lowest X_D and X_B excitons are four exciton states derived from e_1 and h_2. They have degeneracies of 1, 2, and 1 and are, respectively, dark, bright, and bright. Their separation from the lowest (e_1h_1)-derived excitons is of the order of 25–30 meV. We find that, in the single-configuration approximation, $\tau(X_D)$ is in the millisecond range and increases with increasing dot size from 7.7 ms for a $R=10.3$ Å dot to 720 ms for a $R=19.2$ Å dot. Interestingly, in the effective-mass approximation,[14] the lowest-energy exciton is completely dark and therefore has infinite radiative lifetime. As a result, other mechanisms were invoked to explain the observed finite lifetime of the dark exciton.[14] In our pseudopotential calculations, emission from the lowest-energy exciton has finite oscillator strength (and thus finite lifetime) because of the atomistic character of the band-edge single-particle wave functions and the coupling with higher-energy excitonic configurations in the many-body CI Hamiltonian. Recent atomistic calculations[16] have shown that in the presence of surface states, the lowest-energy exciton acquires significant oscillator strength due to the mixing of dark and bright excitonic states.

(4) Inclusion of correlations via configuration interaction (LMT 4) lets (e_ih_j)-derived excitons interact with (e_kh_m)-derived excitons. This leads to a further redshift of the exciton energies, without, however, introducing additional level splittings.[9] The bright exciton lifetime $\tau(X_B)$ increases by a factor of about 2 in a $R=10.3$ Å dot, whereas it remains almost unchanged in the largest dot ($R=19.2$ Å). Interestingly, as we see from Fig. 3(a), the contribution of correlation to the radiative lifetime has opposite signs in small ($R=10.3$ Å and $R=14.6$ Å) and large ($R=19.2$ Å) dots. Correlation effects lead to an increase of $\tau(X_B)$ with E_g (i.e., with decreasing dot size), thus reversing the trend of the LMT 1 theory. The effects of correlation are even more pronounced on the dark exciton radiative lifetimes, leading, for a $R=19.2$ Å NQD, to a 2 orders of magnitude decrease of $\tau(X_D)$, compared to the single-configuration approximation (from 720 to 8.2 ms). In smaller NQDs, correlation effects lead to a less dramatic decrease in the dark-exciton lifetime, yielding $\tau(X_D)=1.5$ ms in a $R=10.3$ Å dot.

C. Reversal of polarization of the dark band-edge monoexciton transition

Perhaps the most impressive effect of correlations is a change of the *polarization* of the dark-exciton transitions as a function of size. At LMT 1, LMT 2, and LMT 3, the dark band-edge excitonic transition [labeled 1 in Fig. 1(a)] is 100% polarized *perpendicular* to the nanocrystal z axis (i.e., the wurtzite c axis). However, correlation effects, introduced via CI at LMT 4, yield a size-dependent decrease of the degree of linear polarization [Eq. (4)] of the dark exciton, leading to an inversion of the polarization for a $R=19.2$ Å NQD, where the dark-exciton transition becomes mainly po-

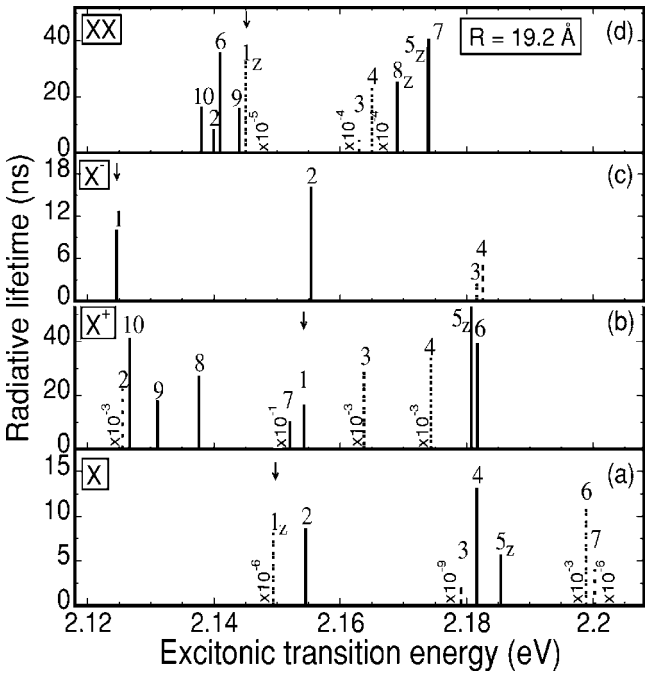

FIG. 4. Radiative lifetimes at zero temperature as a function of emission energy for the various excitonic states considered here. Bright (solid lines) and dark (dashed lines) transitions are labeled according to Fig. 1. The subscript z denotes transitions polarized along the z axis. The arrows mark the position of the fundamental transition (labeled 1 in Fig. 1) from the N-particle ground state to the $(N-2)$-particle ground state.

larized *along* the z axis [Fig. 4(a)]. This effect occurs even when using only three valence states and one conduction state [$N_V=3$ and $N_C=1$ in Eq. (1)] in the expansion of the excitonic wave function, corresponding to a basis set of 12 configurations for X. The bright exciton decay always has perpendicular polarization, as already pointed out by Efros *et al.*[14] A switch of the luminescence polarization alignment with time from parallel to perpendicular to the initial absorbing dipole was observed experimentally by Bawendi *et al.*[17] in 32 Å diameter NQDs. They found that the emission followed a two-component decay, where the slow component (identified as originating from the decay of a dark state) had opposite polarization compared to the fast component (originating from the decay of an optically excited state).

D. Size dependence of the exciton radiative lifetime and comparison with experiment

The scaling of the radiative lifetime with nanocrystal size has been extensively studied and different expressions have been proposed in the literature so far.[14,18,19] Models with various degrees of sophistication, invoked to justify different experimental findings, predict either a decrease[14] or an increase[18,19] of $\tau(X_B)$ with dot size. Among the latter, there is, however, disagreement about the value of the positive exponent γ in the expression $\tau \propto R^{\gamma}$. As discussed above, the size dependence of the radiative lifetime is the result of a competition between two opposite trends when the dot size is reduced: a decrease in the overlap of electron and hole wave

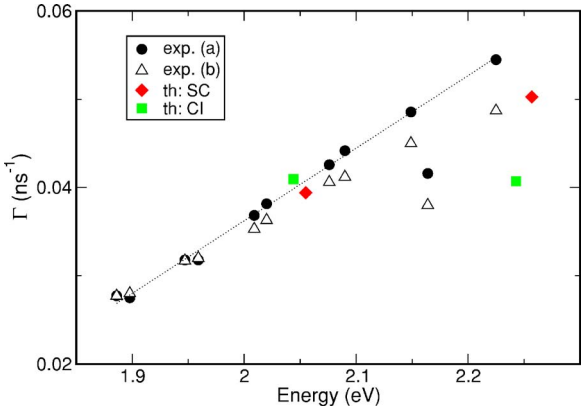

FIG. 5. (Color online) Room-temperature experimental (Ref. 19) PL decay rates deduced from a single exponential fit (black solid circles) and the average arrival time (black open triangles) compared with thermally averaged radiative rates at room temperature $\langle 1/\tau(X)\rangle$ calculated with the semiempirical pseudopotential method in the single-configuration (diamonds) and full-CI (squares) approximations. The dotted line is a linear fit to the solid circles (disregarding the second to the last point), showing that the data points have a linear dependence on the emission energy.

functions (leading to smaller dipole matrix elements $\boldsymbol{M}_{i,j}$) and an increase in the magnitude of the excitonic gap due to increased confinement (leading to larger values of $\omega_{i,j}$).

Recently, van Driel *et al.*,[19] using the fact that the dipole matrix elements are related to the momentum matrix elements by $\langle 0|\boldsymbol{p}|j\rangle = im\omega_j\langle 0|\boldsymbol{r}|j\rangle$, have expressed the rate of spontaneous radiative decay as $\Gamma_j \propto \omega_j|\langle 0|\boldsymbol{p}|j\rangle|^2$. They have then argued that since $\langle 0|\boldsymbol{p}|j\rangle = \langle \mu_c|\boldsymbol{p}|\mu_v\rangle$ (where μ_c and μ_v are the Bloch functions of the conduction and valence bands, respectively), the momentum matrix elements do not depend on the size of the NQD, and therefore $\Gamma_j \propto \omega_j$. Our pseudopotential calculations show that in the single-particle approximation, the momentum matrix elements depend slightly on the NQD size (with a variation of about 7% from a dot with $R=10.3$ Å to one with $R=19.2$ Å). If we take into account the size dependence of the screening factor F in Eq. (2)—which depends on the nanocrystal size via the dielectric constant of the dot—we find that the quantity $P^2 = F|\langle 0|\boldsymbol{p}|j\rangle|^2$ is approximately constant, leading to $\Gamma_j \propto \omega_j$. This result remains valid when excitonic effects are included in the single-configuration approximation (LMT 2 and LMT 3). Our full-CI calculations (LMT 4), however, predict a strong size dependence for P^2, which is found to increase with the nanocrystal radius.

Until recently, no systematic *experimental* study of the size dependence of the radiative decay in CdSe NQDs had been carried out. The trend that could be extrapolated, based on the few available experimental data[20–24] for NQDs of different sizes, was that of a slight *decrease* of the radiative lifetime with increasing dot size. However, a recent experimental paper by van Driel *et al.*[19] showed an increase of the radiative lifetime with size for CdSe quantum dots at room temperature (see Fig. 5, solid circles and empty triangles). The authors interpreted their results in terms of a multilevel model, in which thermal population of optically dark excited

states from a bright ground state is invoked to explain the alleged supralinear dependence of the decay rate with emission frequency.[19] This model, however, does not yield quantitative agreement with experiment, even when resorting to accurate tight-binding calculations of the exciton states which underestimate the decay rate by 75% (Ref. 19). Indeed, it has long been established[9,14] that in CdSe NQDs, the lowest-energy exciton level is *dark*, while the next exciton level (a few meV higher in energy) is *bright* (see Fig. 1(a)). These levels are followed by a multiplet (25–30 meV higher in energy) consisting of one dark and two bright exciton levels.[9,14,15] Therefore, the assumption used in Ref. 19 that the lowest-energy exciton state is bright while higher-energy states are dark appears to oversimplify the exciton electronic structure.

In order to compare our results with the experimental data of van Driel *et al.*,[19] we have calculated the room-temperature thermal average of the radiative rate $\langle \tau(X) \rangle^{-1}$, where the contributions of higher excitonic states were included. We find that the room-temperature radiative lifetime is mainly due to thermal mixing of X_D and X_B. However, as the quantum dot size increases, contributions from higher-energy excitonic states become significant, as these states become closer in energy to X_B. This effect balances the size dependence of the intrinsic lifetime $\tau(X_B)$, yielding similar values for $\langle \tau(X) \rangle$ in both the $R=19.2$ Å and the $R=14.6$ Å dots (the lifetime of the smallest dot is, however, still longer). Our results for the thermally averaged rates in the single-configuration (solid diamonds) and full-CI (solid squares) approximations are compared with the experimental data of van Driel *et al.*[19] in Fig. 5. The single-configuration rates perfectly fit the experimental average arrival time for both dot sizes, whereas the CI rates show better agreement for the larger dot. We note, however, that the overall quantitative agreement with experiment is excellent in this size range, especially considering the poor agreement of both effective-mass approximation and tight-binding calculations.[19] As mentioned above, the difference between single-configuration and full-CI calculations is the inclusion of correlations in the latter. Based on the comparison with the above experimental rates and our calculated single-configuration rates, such inclusion seems to underestimate the dipole matrix elements for the smallest dot considered here [see also Fig. 3(b)].

E. Radiative recombination of biexcitons

The singly degenerate biexcitonic ground state derives from the configuration $(e_1^2 h_1^2)$ [Fig. 1(d)], and is followed, at higher energies, by a dark state derived from $(e_1^2 h_1^1 h_3^1)$. The identity and the optical nature of higher-energy excitonic levels depend on the dot size. In the $R=10.3$ Å dot, the next (third) state derives from $(e_1^2 h_1^1 h_2^1)$ and is bright. It is followed by a dark and by a bright state derived, respectively, from $(e_1^2 h_1^1 h_3^1)$ and $(e_1^2 h_1^1 h_2^1)$. In the $R=14.6$ Å dot, instead, the third state is dark and derives from $(e_1^2 h_1^1 h_3^1)$. Two bright states derived from $(e_1^2 h_1^1 h_2^1)$ follow higher in energy. Similarly, in the $R=19.2$ Å dot, the states above the lowest two singly degenerate levels are dark, bright, and bright, respectively.

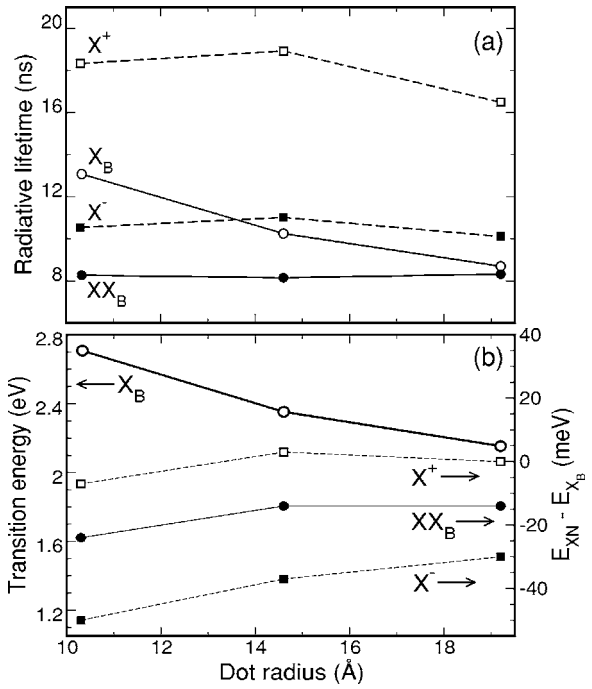

FIG. 6. Size dependence of (a) the radiative lifetime and (b) the corresponding transition energy of the lowest optically allowed transition for X, XX [transitions labeled 2 in Figs. 4(a) and 4(b): solid lines, circles], X^+ and X^- [transitions labeled 1 in Figs. 4(b) and 4(c): dashed lines, squares] at zero temperature. In (b), the transition energies of XX_B, X^+, and X^- are plotted relative to $E(X_B)$.

However, in this case they derive from $(e_1^2 h_1^1 h_3^1)$, $(e_1^2 h_1^1 h_4^1)$, and $(e_1^2 h_1^1 h_2^1)$, respectively.

Figure 4(d) shows our calculated energies, radiative decay times, and polarization for the biexciton transitions labeled 1–10 in Fig. 1(d). Assuming that biexcitons thermalize to the lowest-energy level before recombining, at $T \sim 0$ one would see in emission only transitions from the biexciton ground state to all optically allowed monoexciton levels. However, in Fig. 4(d) we also show lifetimes for transitions from higher biexcitonic states due to their importance in room-temperature emission where higher-energy levels are thermally populated. Interestingly, transition 1 in Fig. 1(d), i.e., the decay from the ground-state biexciton to the ground-state monoexciton, is dark and z polarized, as is the monoexciton band-edge transition [transition 1 in Fig. 1(a)].

The size dependence of both the energy and the radiative lifetime of transition 2 in Fig. 1(d) is shown in Fig. 6. We see that the transition energy is very close to that of X_B for all dot sizes and decreases with increasing dot size. The radiative lifetime is only weakly size dependent, compared to the decrease of the X_B radiative lifetime with increasing size. The ratio of the two lifetimes approaches 2 for the smallest dot and is close to 1 for $R=19.2$ Å. In self-assembled CdSe/ZnSe dots, the ratio $\tau(X_B):\tau(XX_B) \sim 2:1$ was found both in ensemble[25] and in single dot[5] measurements (for dots with exciton emission between 2.25 and 2.38 eV). However, in the latter system, the decay of both exciton and biexciton occurs on a sub-nanosecond time scale at low temperature.

F. Trions

In the trion ground state, the two identical particles are in a spin singlet state, and therefore the trion ground state does not exhibit exchange splitting. The positive trion X^+ [$N=3$ in Fig. 1(b)] shows a bright ground state derived from $(e_1^1 h_1^2)$, followed by three dark states derived from $(e_1^1 h_1^1 h_3^1)$, two dark states derived from $(e_1^1 h_1^1 h_4^1)$, and two bright states derived from $(e_1^1 h_1^1 h_2^1)$. Radiative recombination of X^+ ($N=3$) results in a final state with $N=1$, i.e., a singly occupied hole level h_i. The two lowest-energy states of the negative trion X^- [$N=3$ in Fig. 1(c)] are bright and derive, respectively, from $(e_1^2 h_1^1)$ and $(e_1^2 h_2^1)$. The next two levels are derived from $(e_1^2 h_3^1)$ and $(e_1^2 h_4^1)$ and are dark. X^- decays radiatively into a single electron state e_j.

The zero-temperature transition energies, polarizations, and radiative lifetimes of positive and negative trions are shown in Figs. 4(b) and 4(c), respectively. The size dependence of the energy and radiative lifetime of the lowest trion transition (labeled 1 in Fig. 4) is shown in Fig. 6. We find that while the transition energies of X^- and X^+ are very close, and decrease with increasing nanocrystal size [Fig. 6(b)], the radiative lifetime of X^+ is nearly twice as large as that of X^- [Fig. 6(a)]. We also find that at room temperature, the emission energies of X and X^+ almost coincide for all dot sizes, so it may be difficult to resolve spectroscopically the emission from X^+. However, from Figs. 4 and 6, we see that the emission of both X^- and XX should be detectable as a low-energy shoulder in the PL originating from X, in agreement with recent experimental observations.[4]

IV. CONCLUSIONS

We investigated the properties (lifetimes, transition energies, and polarization) of the radiative emission of monoexcitons, biexcitons, and positive and negative trions in CdSe nanocrystal quantum dots. In the case of the single exciton, we decomposed the final CI results into simple, physically recognizable contributions that derive from increasingly more complex many-body treatments. Our results are in excellent agreement with available experimental data on (i) the size dependence of the exciton lifetime and (ii) the degree of polarization of the decay from the lowest dark monoexciton.

ACKNOWLEDGMENT

This work was funded by the U.S. Department of Energy, Office of Science, Basic Energy Sciences, under Contract No. DE-AC36-99GO1337 to NREL.

[1] V. I. Klimov, A. A. Mikhailovsky, D. W. McBranch, C. A. Leatherdale, and M. G. Bawendi, Science **287**, 1011 (2000).
[2] L. W. Wang, M. Califano, A. Zunger, and A. Franceschetti, Phys. Rev. Lett. **91**, 056404 (2003).
[3] C. Wang, M. Shim, and P. Guyot-Sionnest, Science **291**, 2390 (2001).
[4] M. Achermann, J. A. Hollingsworth, and V. I. Klimov, Phys. Rev. B **68**, 245302 (2003).
[5] B. Patton, W. Langbein, and U. Woggon, Phys. Rev. B **68**, 125316 (2003).
[6] In an exciton with N particles, we define as "bright" ("dark") states that are optically accessible (inaccessible) from the ground state of the excitonic configuration with $(N-2)$ particles.
[7] L. W. Wang and A. Zunger, Phys. Rev. B **53**, 9579 (1996).
[8] L. W. Wang and A. Zunger, Phys. Rev. B **51**, 17398 (1995).
[9] A. Franceschetti, H. Fu, L. W. Wang, and A. Zunger, Phys. Rev. B **60**, 1819 (1999).
[10] D. L. Dexter, *Solid State Physics* (Academic, New York, 1958), Vol. 6, pp. 358–361.
[11] D. R. Lide, *Handbook of Chemistry and Physics*, 79th ed. (CRC, Boca Raton, FL, 1999).
[12] S. F. Wuister, C. de Mello Donegá, and A. Meijerink, J. Chem. Phys. **121**, 4310 (2004).
[13] C. A. Leatherdale, W. K. Woo, F. V. Mikulec, and M. G. Bawendi, J. Phys. Chem. B **106**, 7619 (2002).
[14] Al. L. Efros, M. Rosen, M. Kuno, M. Nirmal, D. J. Norris, and M. Bawendi, Phys. Rev. B **54**, 4843 (1996).
[15] K. Leung, S. Pokrant, and K. B. Whaley, Phys. Rev. B **57**, 12291 (1997).
[16] M. Califano, A. Franceschetti, and A. Zunger, Nano Lett. **5**, 2360 (2005).
[17] M. G. Bawendi, P. J. Carroll, W. L. Wilson, and L. E. Brus, J. Chem. Phys. **96**, 946 (1992).
[18] A. Javier, D. Magana, T. Jennings, and G. F. Strouse, Appl. Phys. Lett. **83**, 1423 (2003).
[19] A. F. van Driel, G. Allan, C. Delerue, P. Lodahl, W. L. Vos, and D. Vanmaekelbergh, Phys. Rev. Lett. **95**, 236804 (2005).
[20] O. Labeau, P. Tamarat, and B. Lounis, Phys. Rev. Lett. **90**, 257404 (2003).
[21] G. Schlegel, J. Bohnenberger, I. Potapova, and A. Mews, Phys. Rev. Lett. **88**, 137401 (2002).
[22] B. Lounis, H. A. Bechtel, D. Gerion, P. Alivisatos, and W. E. Moerner, Chem. Phys. Lett. **329**, 399 (2000).
[23] G. Messin, J. P. Hermier, E. Giacobino, P. Desbiolles, and M. Dahan, Opt. Lett. **26**, 1891 (2001).
[24] S. A. Crooker, T. Barrick, J. A. Hollingsworth, and V. I. Klimov, Appl. Phys. Lett. **82**, 2793 (2003).
[25] F. Gindele, U. Woggon, W. Langbein, J. M. Hvam, K. Leonardi, D. Hommel, and H. Selke, Phys. Rev. B **60**, 8773 (1999).